

Core-shell reconfiguration through thermal annealing in $\text{Fe}_x\text{O}/\text{CoFe}_2\text{O}_4$ ordered 2D nanocrystal arrays

This content has been downloaded from IOPscience. Please scroll down to see the full text.

2014 Nanotechnology 25 055601

(<http://iopscience.iop.org/0957-4484/25/5/055601>)

View [the table of contents for this issue](#), or go to the [journal homepage](#) for more

Download details:

IP Address: 131.180.64.121

This content was downloaded on 13/01/2014 at 09:26

Please note that [terms and conditions apply](#).

Core–shell reconfiguration through thermal annealing in $\text{Fe}_x\text{O}/\text{CoFe}_2\text{O}_4$ ordered 2D nanocrystal arrays

Anil O Yalcin¹, Bart de Nijs², Zhaochuan Fan³, Frans D Tichelaar¹, Daniël Vanmaekelbergh⁴, Alfons van Blaaderen², Thijs J H Vlugt³, Marijn A van Huis² and Henny W Zandbergen¹

¹ Kavli Institute of Nanoscience, Delft University of Technology, Lorentzweg 1, 2628 CJ Delft, The Netherlands

² Soft Condensed Matter, Debye Institute for Nanomaterials Science, Utrecht University, Princetonplein 5, 3584 CC Utrecht, The Netherlands

³ Process and Energy Laboratory, Delft University of Technology, Leeghwaterstraat 44, 2628 CA Delft, The Netherlands

⁴ Condensed Matter and Interfaces, Debye Institute for Nanomaterials Science, Utrecht University, Princetonplein 5, 3584 CC Utrecht, The Netherlands

E-mail: a.o.yalcin@tudelft.nl

Received 7 October 2013, revised 2 December 2013


Accepted for publication 5 December 2013

Published 9 January 2014

Abstract

A great variety of single- and multi-component nanocrystals (NCs) can now be synthesized and integrated into nanocrystal superlattices. However, the thermal and temporal stability of these superstructures and their components can be a limiting factor for their application as functional devices. On the other hand, temperature induced reconstructions can also reveal opportunities to manipulate properties and access new types of nanostructures. *In situ* atomically resolved monitoring of nanomaterials provides insight into the temperature induced evolution of the individual NC constituents within these superstructures at the atomic level. Here, we investigate the effect of temperature annealing on 2D square and hexagonal arrays of $\text{Fe}_x\text{O}/\text{CoFe}_2\text{O}_4$ core/shell NCs by *in situ* heating in a transmission electron microscope (TEM). Both cubic and spherical NCs undergo a core–shell reconfiguration at a temperature of approximately 300 °C, whereby the Fe_xO core material segregates at the exterior of the CoFe_2O_4 shell, forming asymmetric dumbbells ('snowman-type' particles) with a small Fe_xO domain attached to a larger CoFe_2O_4 domain. Upon continued annealing, the segregated Fe_xO domains form bridges between the CoFe_2O_4 domains, followed by coalescence of all domains, resulting in loss of ordering in the 2D arrays.

Keywords: 2D nanocrystal superlattices, colloidal crystals, core–shell nanocrystals, thermal evolution, *in situ* transmission electron microscopy

 Online supplementary data available from stacks.iop.org/Nano/25/055601/mmedia

(Some figures may appear in colour only in the online journal)

1. Introduction

With the development of colloidal nanoscience, it has become possible to synthesize a plethora of single- and multi-component nanocrystals offering novel applications in

chemistry, physics and materials science [1–3]. Metallic clusters and nanocrystals have been used in catalysis already for decades, as the NCs have a high density of active surface sites due to their large surface area to volume ratio. Semiconductor nanocrystals are for instance used in

optoelectronic applications. Their radius is smaller than the exciton radius, which leads to strong quantum confinement and thereby to size-dependent optoelectrical properties [4, 5].

In recent years, much effort has been devoted to colloidal heterosystems: systems that have two compounds (or more) and an interface in between. The presence of the two compounds (metals, semiconductors, magnets) together with the interface opens a tremendous number of new degrees of freedom to tailor the physical properties. Colloidal particles with two semiconductor compounds can show delocalized excitons, for which the lifetime and emission energy can be tailored, which is also important in lasing [6]. Compounds with a metallic/magnetic core and semiconductor shell are important in magnetotransport [7]. Furthermore, FeO_x -type nanoparticles are also used for creating binary nanocrystal superlattices (BNSLs), displaying physical metaproperties. It has been shown that Au/FeO_x binary superlattices can be used as catalysts for carbon monoxide (CO) oxidation [8], while magnetotransport properties have been demonstrated in $\text{Fe}_3\text{O}_4/\text{FePt}$ superlattices [9].

An often undesired property of such nanosystems, though, is their structural instability with respect to heating, even at temperatures far below the melting temperature of the bulk solids. This is of utmost importance, as it may form a hurdle towards industrial applications of these systems, such as in quantum dot solar cells and core-shell NCs used for down-conversion of light in light emitting diodes (LEDs). On the other hand, this could also be used in a beneficial way to manipulate the properties of such structures, such as in alloy formation at low temperatures, or even to make structures otherwise not reachable. For example, it was previously shown that heating can transform ill-defined CdSe/Au interfaces in Au -tipped CdSe nanorods into crystallographically well-defined interfaces [10]. Heating can also induce oriented attachment of NCs [11], which provides opportunities for making two-dimensional semiconductor supercrystals [12, 13]. In other cases, it was demonstrated that a combination of heating and irradiation can transform Au -tipped CdS nanorods into AuS/Cd core-shell NCs [14], and that heating induced transformation of PbSe/CdSe core/shell NCs into attached PbSe/CdSe bi-hemispheres, accompanied by drastic changes in the optical properties [15].

Understanding of the driving forces in these temperature induced structural conversions is limited until now. This also holds for the kinetics and atomic-scale motions during these conversions. One way to acquire more knowledge is by studying model systems using time resolved, atomic resolution *in situ* TEM [16]. Here we study $\text{Fe}_x\text{O/CoFe}_2\text{O}_4$ core-shell nanoparticles as a model system for many complex oxides. This is a relevant system, because FeO_x -type nanoparticles are nowadays frequently used in the fabrication of binary superlattices [8, 9, 17–20]. The advantage of this core-shell system is that it can be synthesized both in spherical and cubical morphologies [21], yielding hexagonal and square 2D superlattices, respectively. Furthermore, the crystal structures of the core and shell material have a good epitaxial fit due to the small difference in lattice parameters.

Within the $\text{Fe}_x\text{O/CoFe}_2\text{O}_4$ core/shell NCs, the Fe_xO core is antiferromagnetic and the CoFe_2O_4 shell is

ferromagnetic [19, 21–24]. Magnetic dipolar interactions in these NCs are reported to have little effect on the superlattice formation [19]. As a bulk phase, the core material Fe_xO ($x = 0.83\text{--}0.95$) [21, 25] is only stable at high temperatures (it decomposes into $\alpha\text{-Fe}_2\text{O}_3$, $\gamma\text{-Fe}_2\text{O}_3$ and Fe_3O_4 below 560°C); however, as a nanocrystal, it is stable at room temperature [21, 22, 26]. The phase is named wüstite, and can be considered a rocksalt phase with a partially occupied cation sublattice. The shell material consists of CoFe_2O_4 , and has a spinel crystal structure. The oxygen sublattices of Fe_xO and CoFe_2O_4 are identical and continuous over the interface, and therefore the $\text{Fe}_x\text{O/CoFe}_2\text{O}_4$ NCs are well-defined, atomically coherent core/shell systems.

Here, we investigate by means of *in situ* heating experiments inside a transmission electron microscope (TEM) the thermal evolution of two superlattices of $\text{Fe}_x\text{O/CoFe}_2\text{O}_4$ core/shell NCs, one being a square array of cubic particles and another being a hexagonal array consisting of spherical particles. In both cases, a striking morphological transformation takes place, whereby the Fe_xO core leaves the shell structure and segregates at the exterior of the shell.

2. Methods

2.1. Synthesis of spherical and cubical NCs

For synthesis of the $\text{Fe}_x\text{O/CoFe}_2\text{O}_4$ NCs the method proposed in [27] was used. For a typical NC synthesis a precursor mixture was prepared by combining 8.66 g $\text{FeCl}_3 \cdot 4\text{H}_2\text{O}$ (32 mmol, Sigma-Aldrich, 99%) dissolved in 80 ml methanol (Sigma-Aldrich, absolute, MeOH) with 2.0 g CoCl_2 (16 mmol, Sigma-Aldrich, >98%) dissolved in 40 ml MeOH. 40.2 g oleic acid (Aldrich, 90%, OA) was added to the mixture. Next, 5.12 g sodium hydroxide (Acros Organics pellets, extra pure) dissolved in 320 ml MeOH was slowly added to the mixture. The resulting brown viscous liquid was retrieved by decanting and washed three times with MeOH. The mixture was dissolved in 80 ml hexane (Aldrich, mixture of isomers), separated using a separatory funnel and washed three times using warm (40°C) de-ionized water (Millipore Direct-Q UV3). The concentration was determined gravimetrically by drying 1 ml of the solution. The solution was diluted to a concentration of 0.5 mol kg^{-1} by adding 1.48 g octadecene (Sigma-Aldrich, 90%, ODE) for each gram of mixed oleate, and the hexane was removed by evaporation. For a typical synthesis of spherical core-shell NCs, 9.6 g precursor solution, 0.76 g OA and 13.70 g ODE were combined and heated to reflux temperature for 40 min under nitrogen. The resulting NCs were isolated by adding 20 ml ethanol (100%, ETOH) and 15 ml of hexane and centrifugation at 4000 rpm for 3 h (using a Hettich Zentrifugen Rotina 46 s), and then redispersed in cyclohexane (Sigma-Aldrich, $\geq 99.8\%$). For a typical synthesis of cubic core-shell NCs, 9.6 g precursor solution, 0.76 g OA, 1.46 g sodium oleate (ABCR, 95%) and 12.50 g ODE were combined and heated to reflux temperature for 40 min, the resulting NCs were isolated by adding 15 ml of hexane and 20 ml of ETOH and centrifugation at 4000 rpm for 3 h, and

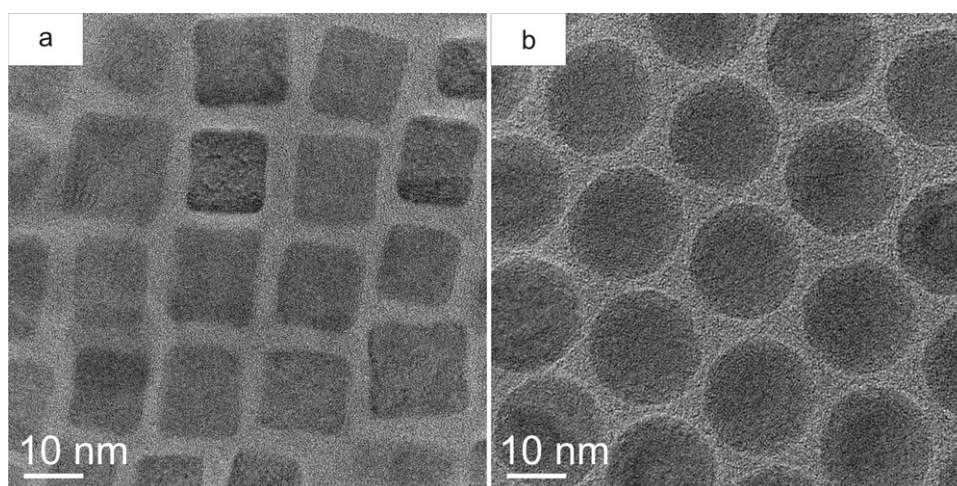


Figure 1. TEM images of different types of 2D arrays. (a) Cubic $\text{Fe}_x\text{O}/\text{CoFe}_2\text{O}_4$ core/shell NCs forming a square 2D array, (b) spherical $\text{Fe}_x\text{O}/\text{CoFe}_2\text{O}_4$ core/shell NCs forming a hexagonal 2D array.

then redispersed in cyclohexane. The NC suspensions were stored under Ar atmosphere.

2.2. *In situ* TEM studies

High-resolution TEM (HRTEM) with aberration correction was used for the imaging to resolve the atomic lattices and study the orientation relationship between the various nanoscale domains. The TEM imaging mode is a fast recording mode (~ 10 frames s^{-1}), which also enables one to record movies of the transformation with good time resolution. High-angle annular dark-field scanning transmission electron microscopy (HAADF-STEM) does not suffer from intensity changes caused by diffraction contrast, and was used to distinguish with more certainty between the Fe_xO and CoFe_2O_4 domains. In this imaging mode, the intensity scales with Z^2 (so-called Z-contrast), where Z is the atomic number of the element. Because of the higher density of the Fe_xO phase with respect to the CoFe_2O_4 phase, the Fe_xO phase appears brighter in the images. Finally, energy-filtered TEM (EFTEM) studies were conducted in order to perform not only density-based imaging, but also chemical mapping of the Co content, whereby the images are energy-filtered by setting an energy window over the characteristic Co peak in the electron energy loss spectrum (EELS).

For TEM studies, 8 μl of solution was dropcast onto a MEMS micro-hotplate (microelectronic mechanical system) inside the glove box. More information about the micro-hotplate and its application in TEM studies can be found in [16]. After the micro-hotplate was mounted in a dedicated TEM specimen holder, this set-up was plasma cleaned for 15 s in order to remove excess solution residues. A Cs aberration corrected FEI Titan microscope operating at 300 kV accelerating voltage was used in *in situ* heating experiments and in HAADF-STEM imaging. EFTEM studies were carried out with an FEI Monochromated Tecnai F20ST.

3. Results

Figure 1 shows the square (figure 1(a)) and hexagonal (figure 1(b)) 2D arrays of cubic and spherical $\text{Fe}_x\text{O}/\text{CoFe}_2\text{O}_4$ core/shell NCs respectively. For the superlattice shown in figure 1(a), the $\{100\}$ atomic lattices were aligned with the axes of the 2D array, which was a direct result of the crystallographic $\{100\}$ facets that were facing each other. In the case of the spherical $\text{Fe}_x\text{O}/\text{CoFe}_2\text{O}_4$ NCs shown in figure 1(b), there was no such facet alignment. Figure 2 shows the overall cubic $\text{Fe}_x\text{O}/\text{CoFe}_2\text{O}_4$ core/shell NC arrays and HRTEM images of single core/shell NCs. The Fe_xO core has a rock salt structure with some cation deficiencies ($x = 0.83\text{--}0.95$) [21, 25] and the lattice constant varies between 4.255 and 4.294 Å depending on the oxidation state [25]. The $\{200\}$ planar distance of Fe_xO was measured as 2.1 Å, consistent with the rock salt structure. The CoFe_2O_4 shell has a spinel crystal structure (lattice constant 8.46 Å [28]). Both structures have a face-centered cubic (fcc) oxygen sublattice with a lattice mismatch of only 3% [21, 25]. The $\{100\}$ surfaces of the NCs were mutually aligned, resulting in a square 2D array.

As the crystal structures of core and shell materials are similar, an objective aperture was inserted to enhance the diffraction contrast (figures 2(a) and (b)). The Fe_xO core material exhibited darker contrast compared to the CoFe_2O_4 shell material in the diffraction contrast images. The diffraction contrast effect is demonstrated more systematically for a single NC in figure S1 of the supporting information (available at stacks.iop.org/Nano/25/055601/mmedia). In figures 2(a) and (b), the core and the shell cannot be distinguished in all the nanocubes since the (diffraction) contrast between the shell and the core depends sensitively on the crystal orientation with respect to the electron beam. As the NCs were not all exactly in the same orientation, the core-shell contrast was not always visible, which was also observed in earlier studies on a very similar system ($\text{Fe}_x\text{O}/\text{Fe}_3\text{O}_4$ wüstite/spinel NCs) [25, 29].

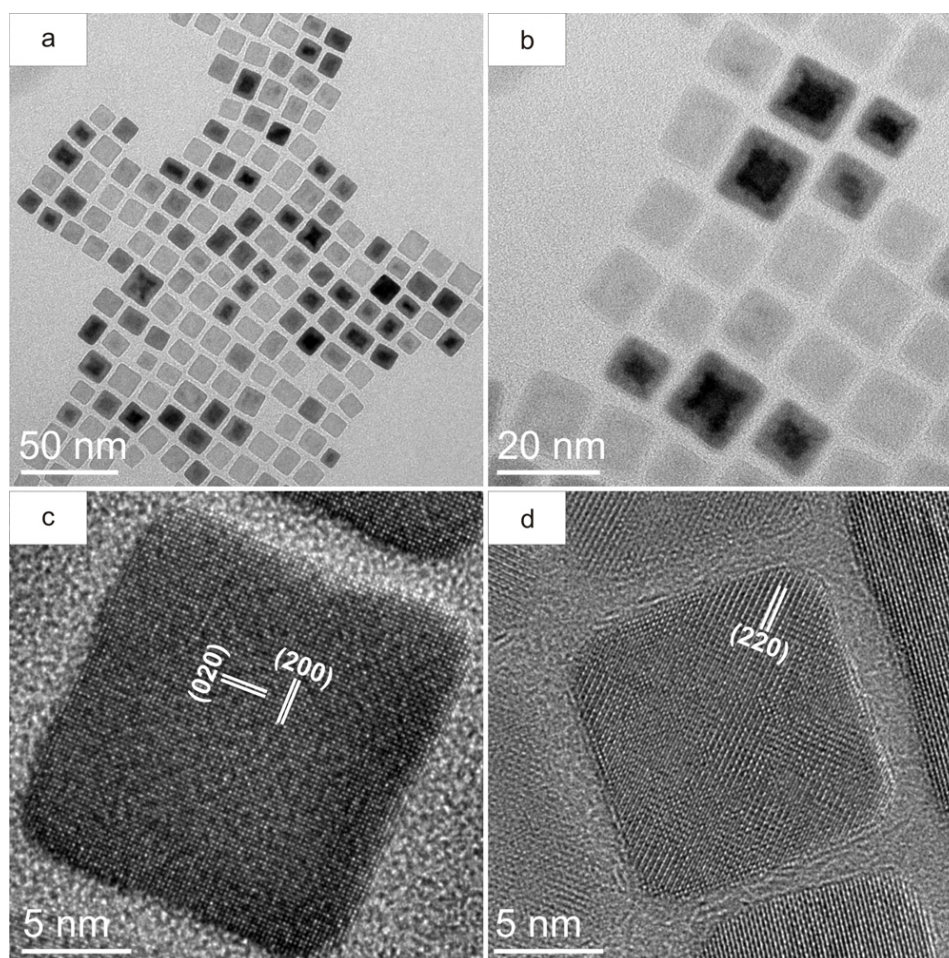


Figure 2. (a) and (b) TEM images (diffraction contrast) of 2D square arrays consisting of cubic $\text{Fe}_x\text{O}/\text{CoFe}_2\text{O}_4$ core/shell NCs. An objective aperture was inserted to enhance the diffraction contrast between the Fe_xO and the CoFe_2O_4 materials. (c) and (d) HRTEM images of cubic core/shell NCs. The observed lattice spacings were 2.1 Å, corresponding to the (200) lattice spacing of the Fe_xO core and 3.0 Å corresponding to the (220) lattice spacing of the CoFe_2O_4 shell.

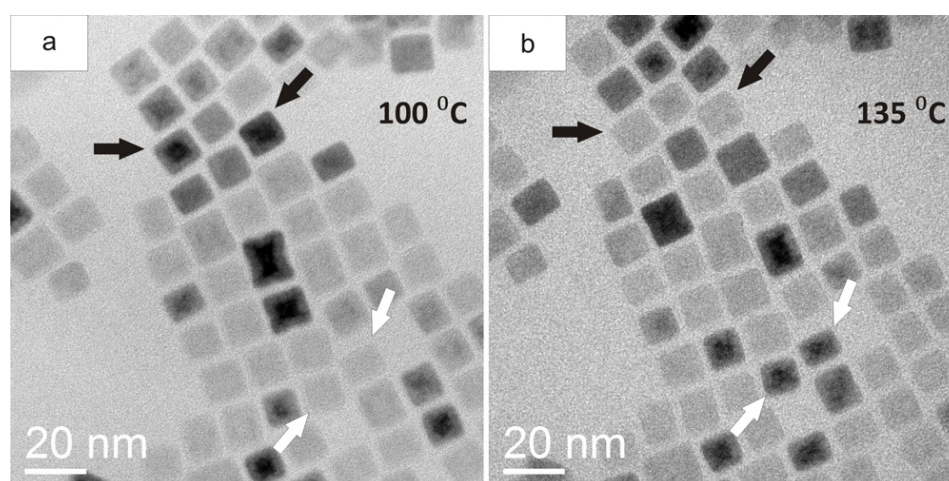


Figure 3. TEM images (diffraction contrast) of a square $\text{Fe}_x\text{O}/\text{CoFe}_2\text{O}_4$ core/shell 2D NC array at (a) 100 °C and (b) 135 °C. The black arrows show NCs, whereby the core could be distinguished at 100 °C while it could no longer be distinguished at 135 °C. The white arrows show NCs where the opposite occurred.

Figure 3 shows the square array at 100 and 135 °C. It is clear from the images that during heating some NCs changed their alignment with respect to the electron beam, so that in

certain cases the core-shell contrast appeared (indicated with white arrows in figures 3(a) and (b)) while in other cases it disappeared (indicated with black arrows in figures 3(a)

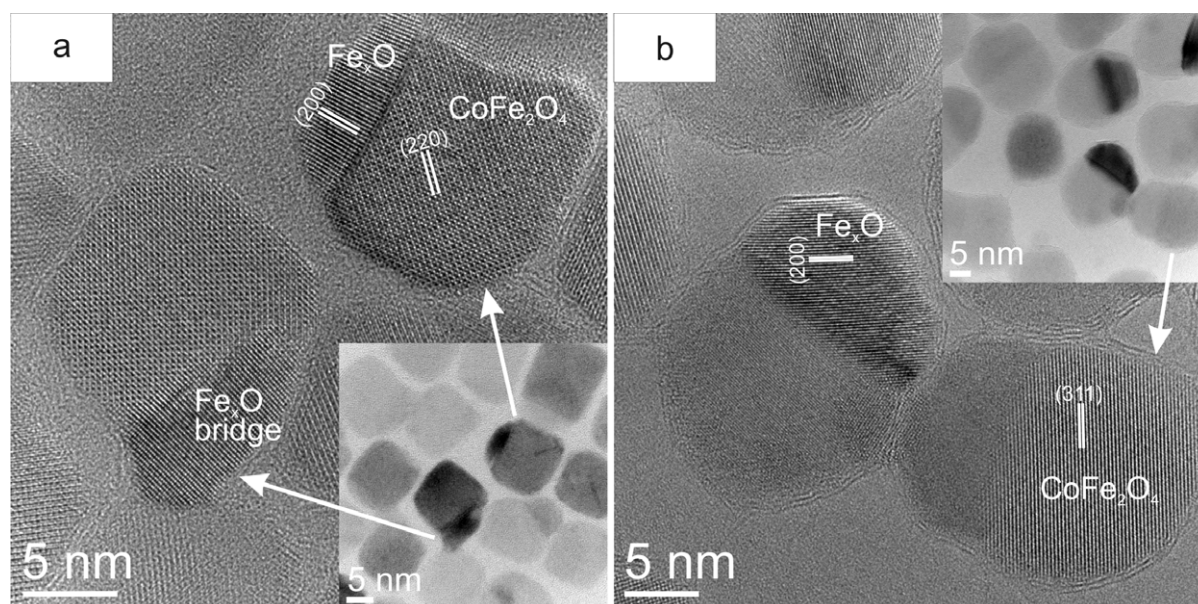


Figure 4. TEM images of Fe_xO/CoFe₂O₄ ‘initially’ core/shell NC arrays; (a) cubic NCs at 335 °C and (b) spherical NCs at 360 °C. The insets in the images were taken when the objective aperture was inserted (diffraction contrast). The (200) spacing of Fe_xO is 2.1 Å, and the (220) and (311) spacings of CoFe₂O₄ are 3.0 Å and 2.55 Å respectively.

and (b)). In the supporting movie M1 (available at stacks.iop.org/Nano/25/055601/mmedia), an example of the contrast (diffraction) change is shown due to changes in the alignment of NCs with respect to the electron beam with changing temperature.

With a heating rate of 10° min⁻¹, a reconfiguration of the core and shell materials was observed at a temperature of 300 °C, as shown in figure 4. The hexagonal arrays exhibited reconfiguration at a slightly higher temperature (320 °C) than the square arrays. During the reconfiguration, the Fe_xO core material left the CoFe₂O₄ shell in both square and hexagonal NC arrays and segregated at the exterior of the shells, thereby forming asymmetric dumbbells (‘snowman-type’ particles). Subsequently, Fe_xO domains formed bridges between the CoFe₂O₄ materials, as shown in figure 4(a). The CoFe₂O₄ shells of cubic NCs also underwent a slight reconfiguration in which they became more rounded at the edges. Eventually also these domains coalesced at higher temperatures, resulting in loss of ordering of the 2D NC arrays. The reconfiguration was observed subsequently at other regions (not previously in the field of view) on the substrate, therefore it can be concluded that the electron beam does not have a strong influence on the reconfiguration or the reconfiguration temperature. More images showing the reconfiguration of NCs at different locations can be found in figure S2 in the supporting information (available at stacks.iop.org/Nano/25/055601/mmedia). Furthermore, supporting movies M2, M3 and M4 (available at stacks.iop.org/Nano/25/055601/mmedia) show the reconfiguration and segregation of the Fe_xO core material. Diffraction contrast was used in movies M2 and M3 (available at stacks.iop.org/Nano/25/055601/mmedia), in which the reconfiguration of the Fe_xO core was clearly observed. Supporting movie M4 (available at stacks.iop.org/Nano/25/055601/mmedia)

is a HRTEM movie of the reconfiguration of Fe_xO forming a bridge between two cubic NCs.

High-angle annular dark-field scanning transmission electron microscopy (HAADF-STEM) studies confirmed the reconfiguration of these NCs. In HAADF-STEM studies, collection angles above 30 mrad exhibit Z-contrast imaging and diffraction effects can be minimized [30]. Thus, a small camera length (183 mm) was employed to ensure that electrons scattered beyond 30 mrad were used in HAADF-STEM studies [31, 32]. In the CoFe₂O₄ structure, 75% of the cation sites are occupied and in the case of the Fe_xO structure, 83–95% of the cation sites are occupied [21, 25]. As a result, the Fe_xO structure exhibited brighter contrast in comparison to CoFe₂O₄ in the HAADF-STEM images. Figure 5 shows cubic NCs during heating. The insets show the intensity profiles along the white rectangles in the HAADF-STEM images. From room temperature (RT) to 300 °C (figure 5(b)), the NCs became rounded, showing that the morphology of the CoFe₂O₄ shell also changed. In the NC indicated with a white arrow in figure 5, the Fe_xO contrast was apparent initially (inset in figure 5(a)) and core-shell contrast was lost with increasing temperature (figures 5(b)–(f)). At 350 °C (figure 5(d)), the Fe_xO—most likely from two cores—formed a bridge with the neighboring NC. The smooth intensity profiles along the NC at elevated temperatures (figures 5(d)–(f)) suggest that the CoFe₂O₄ shell material filled up the core volume during reconfiguration. The NC shape became more irregular at temperatures above 380 °C (figures 5(e) and (f)).

Energy-filtered TEM (EFTEM) studies in figure 6 showed that heated Fe_xO domains contained Co as well. Prior to the EFTEM experiments, initially spherical NCs

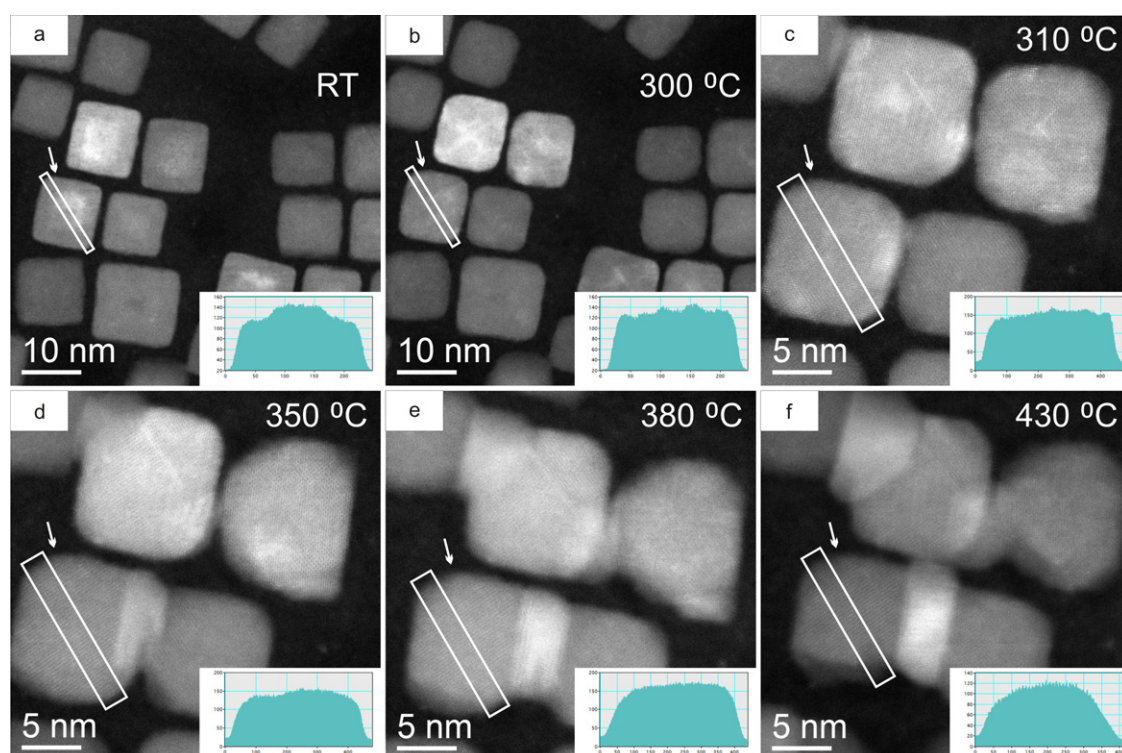


Figure 5. HAADF-STEM images of cubic $\text{Fe}_x\text{O}/\text{CoFe}_2\text{O}_4$ NCs. The insets are intensity profiles taken from the white rectangles in the images. (a) NCs at room temperature (RT) before reconfiguration. The Fe_xO core exhibited brighter contrast compared to the CoFe_2O_4 shell. (b)–(f) NCs at 300 °C, 310 °C, 350 °C, 380 °C and 430 °C respectively. The cubic NCs became rounded and the intensity variation at the core region was lost ((b)–(f)), suggesting filling of the core volume by the CoFe_2O_4 shell material. The NC shape became more irregular at temperatures above 380 °C ((e) and (f)). HAADF-STEM images were taken with a camera length of 183 nm and a dwell time of 130 μs .

were further heated to 530 °C to obtain bigger domains of Fe_xO and CoFe_2O_4 . With elemental mapping of Co ($L_{2,3}$ edge at 779 eV), the domains containing Co gave contrast. Figures 6(a) and (c) are the zero-loss images and figures 6(b) and (d) are the corresponding Co maps respectively. Dotted lines were used to emphasize the Fe_xO domains (dark contrast in zero-loss images). The arrows show Fe_xO domains with the presence of Co (weak contrast in Co maps). In a recent study, Sytnyk *et al* [33] showed that Co can diffuse in the Fe_xO wüstite structure, which explains the weak contrast of the Fe_xO domains in the Co maps. Note that annealing at an elevated temperature (530 °C) can also play a role in the presence of Co in the Fe_xO domains, as temperature enhances the solubility and diffusivity of species.

4. Discussion

In the synthesis of the spherical core/shell NCs, oleic acid was used as the main ligand, while in the case of cubic core/shell NCs, a mixture of sodium oleate and oleic acid was used [21]. It has been reported that the presence of sodium oleate hinders the growth rate in the $\langle 100 \rangle$ direction, and as a result the cubic shape is favored over spherical [21]. In cubic core/shell NCs, the surfaces consist of $\{100\}$ facets, and individual NCs can easily align their $\{100\}$ facets with respect to each other, resulting in the formation of a square 2D array. Spherical NCs with mostly hard interactions tend to form cubic (fcc) and

hexagonal superlattices [24], whereby magnetic NCs prefer a hexagonal superlattice [34], but can also form body-centered tetragonal superlattices [35].

The reconfiguration in cubic NCs starts at 300 °C and in spherical NCs at a slightly higher temperature (320 °C). Ayyappan *et al* [36] observed (through mass spectroscopy under Ar atmosphere) that oleic acid ligands remain attached to the CoFe_2O_4 NCs up to a temperature of 420 °C, which is higher than the reconfiguration temperature we found. During reconfiguration, the HAADF-STEM and EFTEM images (figures 5 and 6) suggest that Co^{2+} cations diffuse from the shell to the core. Hence, Fe cations (valence Fe^{2+} in Fe_xO and Fe^{3+} in CoFe_2O_4) diffuse to the sides of the NC. The excess of Fe cations in the shell material eventually leads to segregation of Fe_xO domains towards the sides of the NCs. As the core and shell materials have an fcc anion (oxygen) sublattice with a lattice mismatch of only 3% [21, 25], the oxygen sublattice at the core remains unaffected initially, although displacements of O atoms do occur later with the formation of the Fe_xO side domains. The ligands attached to the shell material can play a role in the stabilization of the overall shape during the initial stages of the reconfiguration, thus only slight rounding at the edges is observed (figures 5(b) and (c)). Further annealing, probably accompanied by loss of the ligands, eventually leads to agglomeration (figures 5(d)–(f) and 6) whereby the 2D ordering in the NC arrays is lost. It is also important to note the presence of Co traces in Fe_xO domains (figure 6) at an

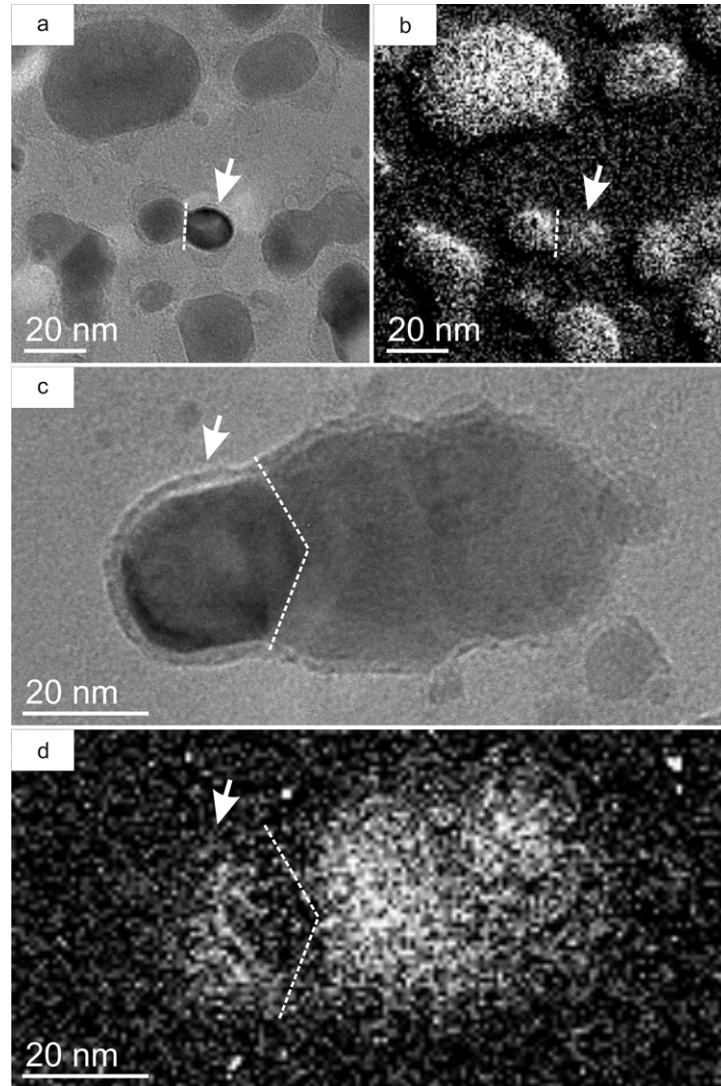


Figure 6. EFTEM Co-mapping of initially spherical NCs. The structure was heated to 530 °C to have bigger domains of individual species. (a) and (c) are the zero-loss images and (b) and (d) are the corresponding Co maps of them respectively. The $L_{2,3}$ edge of Co is at 779 eV. Fe_xO domains exhibited dark contrast in zero-loss images. The dotted lines were used to clarify these domains. EFTEM studies revealed that heated Fe_xO domains contained Co. Arrows show the Fe_xO domains with the presence of Co. A slit width of 20 eV was used in the EFTEM studies.

elevated temperature (530 °C), which is probably triggered by temperature enhanced diffusivity. The electron beam does not have a substantial effect on the reconfiguration behavior or the reconfiguration temperature, as this phenomenon was observed everywhere on the substrate.

It is clear that the asymmetric dumbbell ('snowman-type' particle) arrangement with the Fe_xO domain at the exterior of the $CoFe_2O_4$ shell constitutes a lower energy configuration than the core-shell one present before annealing. As a first approximation (neglecting nano-size effects, edge and corner effects, magnetic effects), the total free energy G of the system can be written as

$$G = \sum g_i^{\text{bulk}} V_i + \sum \gamma_{ij} A_{ij} \quad (1)$$

where g_i^{bulk} is the Gibbs free energy per unit volume of bulk phase i , and γ_{ij} is the interface energy or surface tension at

any interface between media i and j , including solid-solid, solid-ligand, and any interface with gas or vacuum.

Considering this energy balance in view of the experimentally observed core-shell reconfiguration, we note that (1) a Fe_xO surface is created where it did not exist beforehand; (2) the interfacial area between Fe_xO and $CoFe_2O_4$ is strongly reduced; and (3) the surface area of $CoFe_2O_4$ has changed: it decreased at the exterior where the Fe_xO domain is now attached. It seems likely that the decrease in the interfacial area between Fe_xO and $CoFe_2O_4$, together with the decrease in the surface area of $CoFe_2O_4$, brings a lower total energy despite the creation of a Fe_xO surface. A very similar transformation was found previously for $PbSe/CdSe$ core/shell particles, which transformed into $PbSe/CdSe$ bi-hemispheres [15].

The core/shell reconfiguration in the NCs as well as the loss of ordering in the 2D arrays raise concerns about the

application of these NCs in possible devices. The current results indicate that the thermal stability (and thus also the temporal stability) of these NC arrays is limited. Considering their chemical stability, it has been reported that for a similar structure of cubic $\text{Fe}_x\text{O}/\text{Fe}_3\text{O}_4$ core/shell NCs, air oxidation at room temperature leads to transformation of the Fe_xO wüstite core to the spinel Fe_3O_4 structure [25]. In addition, annealing CoFe_2O_4 NCs at 400–500 °C in a gas atmosphere (mixture of 93% Ar and 7% H_2) leads to reduction of NCs to FeCo domains [37].

Considering possible implementation of this system in a device/application, the exchange bias effects between the antiferromagnetic Fe_xO core and the ferromagnetic CoFe_2O_4 shell material are of critical importance [21, 25, 33]. The Néel temperature (T_N) of Fe_xO lies around 200 K and the blocking temperature (T_B) of the $\text{Fe}_x\text{O}/\text{CoFe}_2\text{O}_4$ core/shell NC system can vary between 160 and 165 K, making this system superparamagnetic at room temperature [21, 24, 38]. In fact, the blocking temperature depends on the size of the nanocrystal as well as the volumetric ratios of core and shell material [25, 38]. Therefore, the magnetic properties of this system can be manipulated through adjusting the NC size and the core–shell volume fractions. NCs after reconfiguration by thermal annealing can exhibit different exchange bias properties from the original core/shell system through Fe_xO bridge formation between separate NC domains (figure 4(a)) as well as through core volume filling by the shell material (figure 5), and therefore the heating of nanocrystal arrays could be explored as a new technique for the manipulation of the magnetic properties for future applications.

5. Conclusion

The thermal stability of $\text{Fe}_x\text{O}/\text{CoFe}_2\text{O}_4$ core/shell NCs ordered in 2D arrays was investigated by *in situ* heating experiments using TEM. Square 2D arrays of cubic NCs and hexagonal 2D arrays of spherical NCs were investigated. In both systems, a core–shell reconfiguration takes place at a temperature of approximately 300 °C. HRTEM, HAADF-STEM and EFTEM studies confirm that the Fe_xO core material segregates in a domain outside the CoFe_2O_4 shell, thereby forming anisotropic asymmetric dumbbells ('snowman-type' particles) having a well-defined interface. During reconfiguration, the CoFe_2O_4 shell material fills up the core volume and the cubic NCs become more rounded. Upon continued annealing, the segregated Fe_xO domains form bridges between the CoFe_2O_4 domains, followed by further agglomeration of all domains and loss of ordering in the 2D NC arrays. Annealed Fe_xO domains contain Co traces as well. Most likely, the energy gain associated with the decrease in interfacial area is the driving force behind the transformation.

Acknowledgments

This work is part of the research programme of the Foundation for Fundamental Research on Matter (FOM), which is part of the Netherlands Organization for Scientific Research (NWO). MvH acknowledges NWO for a VIDI Grant.

References

- [1] Yin Y and Alivisatos A P 2005 *Nature* **437** 664–70
- [2] Cozzoli P D, Pellegrino T and Manna L 2006 *Chem. Soc. Rev.* **35** 1195–208
- [3] de Mello Donegá C 2011 *Chem. Soc. Rev.* **40** 1512–46
- [4] Alivisatos A P 1996 *Science* **271** 933–7
- [5] Klimov V I, Mikhailovsky A A, Xu S, Malko A, Hollingsworth J A, Leatherdale C A, Eisler H-J and Bawendi M G 2000 *Science* **290** 314–7
- [6] Klimov V I, Ivanov S A, Nanda J, Achermann M, Bezel I, McGuire J A and Piryatinski A 2007 *Nature* **447** 441–6
- [7] Lee J-S, Bodnarchuk M I, Shevchenko E V and Talapin D V 2010 *J. Am. Chem. Soc.* **132** 6382–91
- [8] Kang Y et al 2013 *J. Am. Chem. Soc.* **135** 1499–505
- [9] Dong A, Chen J, Vora P M, Kikkawa J M and Murray C B 2010 *Nature* **466** 474–7
- [10] Figuerola A, van Huis M, Zanella M, Genovese A, Marras S, Falqui A, Zandbergen H W, Cingolani R and Manna L 2010 *Nano Lett.* **10** 3028–36
- [11] van Huis M A, Kunneman L T, Overgaag K, Xu Q, Pandraud G, Zandbergen H W and Vanmaekelbergh D 2008 *Nano Lett.* **8** 3959–63
- [12] Schliehe C et al 2010 *Science* **329** 550–3
- [13] Evers W H, Goris B, Bals S, Casavola M, de Graaf J, van Roij R, Dijkstra M and Vanmaekelbergh D 2013 *Nano Lett.* **13** 2317–23
- [14] van Huis M A, Figuerola A, Fang C, Béché A, Zandbergen H W and Manna L 2011 *Nano Lett.* **11** 4555–61
- [15] Grodzińska D, Pietra F, van Huis M A, Vanmaekelbergh D and de Mello Donegá C 2011 *J. Mater. Chem.* **21** 11556–65
- [16] van Huis M A, Young N P, Pandraud G, Creemer J F, Vanmaekelbergh D, Kirkland A I and Zandbergen H W 2009 *Adv. Mater.* **21** 4992–5
- [17] Talapin D V, Shevchenko E V, Bodnarchuk M I, Ye X, Chen J and Murray C B 2009 *Nature* **461** 964–7
- [18] Redl F X, Cho K-S, Murray C B and O'Brien S 2003 *Nature* **423** 968–71
- [19] Bodnarchuk M I, Kovalenko M V, Pichler S, Fritz-Popovski G, Hesser G and Heiss W 2009 *ACS Nano* **4** 423–31
- [20] Shevchenko E V, Talapin D V, Kotov N A, O'Brien S and Murray C B 2006 *Nature* **439** 55–9
- [21] Bodnarchuk M I, Kovalenko M V, Groiss H, Resel R, Reissner M, Hesser G, Lechner R T, Steiner W, Schäffler F and Heiss W 2009 *Small* **5** 2247–52
- [22] Glaria A, Kahn M L, Chaudret B, Lecante P, Casanove M-J and Barbara B 2011 *Mater. Chem. Phys.* **129** 605–10
- [23] Vanmaekelbergh D 2011 *Nano Today* **6** 419–37
- [24] Bodnarchuk M I, Kovalenko M V, Heiss W and Talapin D V 2010 *J. Am. Chem. Soc.* **132** 11967–77
- [25] Pichon B P et al 2011 *Chem. Mater.* **23** 2886–900
- [26] Yin M, Chen Z, Deegan B and O'Brien S 2007 *J. Mater. Res.* **22** 1987–95
- [27] Kovalenko M V, Bodnarchuk M I, Lechner R T, Hesser G, Schäffler F and Heiss W 2007 *J. Am. Chem. Soc.* **129** 6352–3
- [28] Song Q and Zhang Z J 2004 *J. Am. Chem. Soc.* **126** 6164–8
- [29] Hai H T, Yang H T, Kura H, Hasegawa D, Ogata Y, Takahashi M and Ogawa T 2010 *J. Colloid Interface Sci.* **346** 37–42
- [30] Weyland M, Thomas J M, Dunin-Borkowski R E and Midgley P A 2001 *Inst. Phys. Conf. Ser.* **168** 107–10 EMAG 2001

- [31] Grieb T, Müller K, Fritz R, Schowalter M, Neugebohrn N, Knaub N, Volz K and Rosenauer A 2012 *Ultramicroscopy* **117** 15–23
- [32] Grieb T, Müller K, Fritz R, Grillo V, Schowalter M, Volz K and Rosenauer A 2013 *Ultramicroscopy* **129** 1–9
- [33] Sytnyk M *et al* 2013 *Nano Lett.* **13** 586–93
- [34] Talapin D V, Shevchenko E V, Murray C B, Titov A V and Král P 2007 *Nano Lett.* **7** 1213–9
- [35] Disch S, Wetterskog E, Hermann R P, Salazar-Alvarez G, Busch P, Brückel T, Bergström L and Kamali S 2011 *Nano Lett.* **11** 1651–6
- [36] Ayyappan S, Panneerselvam G, Antony M P and Philip J 2011 *Mater. Chem. Phys.* **130** 1300–6
- [37] Poudyal N, Chaubey G S, Rong C-B, Cui J and Liu J P 2013 *Nanotechnology* **24** 345605
- [38] Hai H T, Kura H, Takahashi M and Ogawa T 2011 *J. Phys.: Conf. Ser.* **266** 012127